2007-6309

AIAA Atmospheric Flight Mechanics Conference and Exhibit, August 20 - 22, Hilton Head, SC

Uncertainty Quantification of the Goland$^+$ Wing's Flutter Boundary

Mohammad Kurdi,* Ned Lindsley,† and Philip Beran‡

Air Force Research Laboratory, WPAFB OH 45433.

Accurate numerical prediction of flutter boundary for fighter aircraft is of great importance. Existing models are deterministic, and do not allow for inherent variations in the system parameters. These variations (e.g. structural dimensions, aerodynamic flow field, stores properties) propagate to uncertainty in the model predictions. In this paper we examine variations in structural dimensions of a "heavy" version of the Goland wing on the flutter boundaries. Initially, the large number of random quantities (component thicknesses and areas) are efficiently reduced by conducting a sensitivity analysis of the baseline wing. Next, an optimization study is carried out to provide a design of the wing that maximizes its first natural frequency while constraining the frequency of the remaining nine modes to no less than their baseline wing counterpart values. The sensitivity study enables selection of a random variable set of the wing components having significant impact on the wing natural frequencies. Monte Carlo simulation is used to propagate the variation in the dimensional properties of the selected set of random quantities of the designed wing. The effect of correlation between random variables is considered. A modal analysis of each realization is evaluated using MSC.Nastran. Flutter boundaries of the propagated sample are predicted based on linear aerodynamic theory (ZAERO®), resulting in a "banded" stability boundary. Results indicate the high sensitivity of the flutter speed to small changes in the structure with an apparent switching in the failure modes.

Nomenclature

A	area of 1-D finite element	ft^2
K	total number of 2-D finite elements	
M	total number of 1-D finite elements	
N	number of realizations	
T	thickness of 2-D finite element	ft
U	free stream air velocity	ft/sec
$\bar{U}_F$	mean flutter speed	ft/sec
$\vec{X}$	set of design variables	
a	factor used to set the design variables side constraints	
c	length in chord wise direction	ft
c_{off}	offset in leading edge of store upstream of the wing leading edge	ft
cg	center of gravity	
f_1	natural frequency of first mode	Hz
k	reduced frequency	
l	length in span wise direction	ft
x, y, z	physical coordinates (stream wise, span wise, vertical)	ft

*NRC Research Associate, AFRL/VASD, 2210 8th Street, Bldg 146, WPAFB, OH 45433. Mohammad.Kurdi@wpafb.af.mil.
†Research Engineer, AFRL/VASD.
‡Principal Research Aerospace Engineer, AFRL/VASD. AIAA Associate Fellow.

Subscripts

d	refers to designed wing
i	finite element number
m	natural mode number
b	refers to baseline wing
s	refers to store property
w	refers to wing property

Conventions

ZONA6 unsteady panel method for subsonic aerodynamics

Symbols

μ	mean
ρ	coefficient of variation $= \sigma/\mu$
σ	standard deviation

I. Introduction

Development of a safe, cost-efficient framework for certification of flutter-free aircraft is highly desirable. Computational aeroelastic methods of varying fidelity provide the necessary tools for predicting flutter boundaries at different flight speeds. Complicating the prediction of flutter speed is variability inherent to the physical model. There is a challenge in propagating these variations through a deterministic aeroelastic model to achieve a representation of variability in the flutter prediction. While representing a challenge, though, deterministic predictions of flutter speed do not represent reality and motivates development of an uncertainty quantification framework that would enable risks within design and certification processes to be quantified.[1]

Aerodynamic modeling fidelity is highly dependent on operating Mach number of the air vehicle. In the subsonic flight regime, linear aerodynamic methods are capable of predicting the flutter boundaries. In the transonic regime, the existence of shock wave on the wing surface complicates the fluid flow solution.[2] In this case nonlinearities in the flow equation have to be considered to provide accurate prediction of transonic flutter.[3] Current methods however use linear aerodynamics to predict regions susceptible to LCOs, where time-marching methods are then used to compute the response by modeling the unsteady behavior of the flow using transonic small disturbance equation[4] or Euler equations.[5] In these methods, extensive analysis is needed to accurately bracket the Hopf point. In our analysis, we use paneling methods based on linearized small disturbance equations,[6] time-linearized small disturbance equations coupled with high fidelity CFD solution of steady background flow field and higher fidelity time-marching method based on complete transonic small disturbance equation.[4] The reader should note that only the last method is capable of computing the LCO time response.

When quantifying uncertainties it is important to consider correlations of parameters. Ignoring this correlation can give a false estimation of the computed variability. Several authors have recognized importance of correlation. Honda and Antonsson[7] accounted for parameter correlation in a multi-criteria design which aggregates performance and design preferences. Becerra and Hernandez[8] regarded physical correlation between parameters necessary in the accurate quantification of uncertainty in air density. In a recent study, Kurdi et al.[9] computed the variability of the stability boundary in milling with and with no correlation. The authors show that when correlation is considered, the output variability was reduced by as much as 50% with a minimum reduction of 10%, whilst providing better agreement with experimental results. In our study, to enable a more accurate calculation of the performance variability, we account for inherent dependencies of random variables.

Uncertainty quantification of aeroelastic stability has received considerable attention see for example the review by Pettit 10 and references therein. Quantifying the variations in the stability response enable a reliable-based design of aircraft structures [11]. Possible sources of variation in the flutter boundary are variations in structural dimensions, aerodynamic flow field and store properties. In this paper we restrict attention to the modeling variations in the structural dimensions of the Goland$^+$ wing. The structural variations are applied to the element sizes (thicknesses of 2-dimensional elements and areas of 1-dimensional elements) of the wing's finite element model. Sensitivity analysis of the wing dimensions is carried out to identify wing elements with high sensitivity to variations in the frequencies of natural modes. Monte

Carlo method is used to propagate the variations to arrive at a probability distribution (histogram) of the flutter speed for different Mach numbers in an unmatched computation. The linear aeroelastic analysis tool ZAERO® is used to perform the analysis. To mimic physical variations, the same random variable is assigned to all the elements of a typical wing component. The probability distribution of the flutter boundary for the propagated sample is examined for different flight regimes. Two nominal configurations of the Goland$^+$ wing are analyzed with store mass and without. High level of sensitivity is observed for the configuration with store mass.

II. Problem Formulation

The wing studied herein is derived from the "heavy" version of the original Goland wing. Like the original, the heavy wing is structurally represented by a beam, but with additional non-structural mass, as defined by Eastep and Olsen.[12] This latest version, referred to as the Goland$^+$ wing,[13] is a heavy wing modeled with a box structure to enable a variety of store attachment options.

II.A. Geometry and Structure

The Goland$^+$ wing is rectangular (Figure 1). Full details of the wing geometry, airfoil shape and properties are given in ref. 13. The wing box finite element model is shown in Figure 1b with overall dimensions of the wing given in Table 1. The wing is composed of 3 spars and 11 ribs with thicknesses and areas of the 1- and 2-D elements of the baseline wing listed in Table 2. The structural elements are given negligible density, thereby decoupling the mass and stiffness properties of the wing. Concentrated masses are added to account for the wing's inertial properties.

A configuration of the wing is examined with an additional tip store mass. The location of the tip store is selected so as to create a hump mode based on linear theory.[14] The existence of this hump mode is a well-known characteristic of LCO behaviors. A store structure attached to the wing tip is used to locate the store mass of 22.496 slugs and is placed at the streamwise, lateral and vertical centers (i.e., x= 0.25 ft, y = 20.5 ft and z = 0 ft). This places the store 1.75 feet forward of the elastic axis, as shown in Figure 1a.

Table 1. Geometric dimensions of wing in feet.

c_w	l_w	c_s	l_s
6	20	10	1

II.B. ZAERO® Aerodynamic Model

Aerodynamic computations of the flutter boundary are facilitated through ZAERO® software. The flutter boundary is computed using the ZONA6 module, which is an unsteady panel method, which solves the three-dimensional linearized small disturbance equations of subsonic aerodynamics.[6] In ZONA6, an aerodynamic model of the wing is established by dividing the wing into panels using the CAERO7 bulk data card with 21 span wise and 39 chord wise grid points. Figure 2a shows the resulting 20 × 38 aerodynamic panels. The fluid/structure interaction is modeled using the 3D spline module in ZAERO®, where the infinite-plate spline method[15,16] is used to transfer the forces and displacements between the structural and aerodynamic models. This enables the aeroelastic analysis of the ensemble of structural variations of the finite element model.

III. Uncertainty Quantification

In this section we describe the details of the uncertainty quantification process. After describing dependence of key parameters, sensitivity and optimization studies are carried out to reduce the number of random variables and provide another design of the wing. The Monte Carlo simulation method is then used to propagate these variations of the baseline and designed wing through the MSC.Nastran finite element models, creating 1000 modal representations per wing. These modal ensembles are then coupled with the ZONA6 aerodynamic model.

]

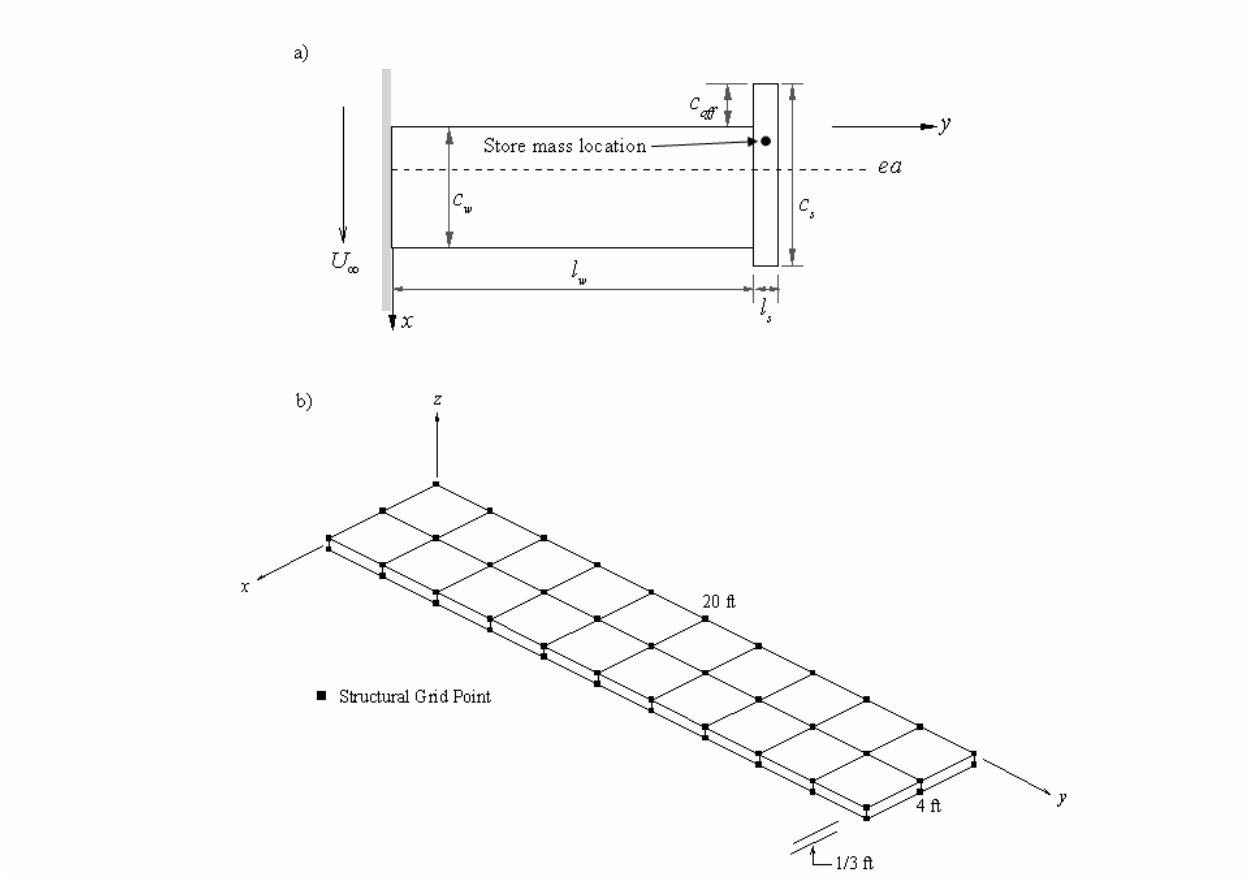

Figure 1. Schematics of Goland$^+$ Wing geometry and structural model: (a) planform geometry; (b) structural model.

Table 2. Thicknesses and areas of finite element components for the baseline wing.

component	2-D element thickness, ft	component	1-D element area, ft^2
upper wing skin	0.0155	posts	0.0008
lower wing skin	0.0155	leading edge spar cap†	0.0416
leading edge spar	0.0006	trailing edge spar cap†	0.0416
trailing edge spar	0.0006	center spar cap†	0.1496
center spar	0.0889	rib cap‡	0.0422
rib	0.0347		

† Dimension for lower and upper spar caps.
‡ Dimension for lower and upper rib caps.

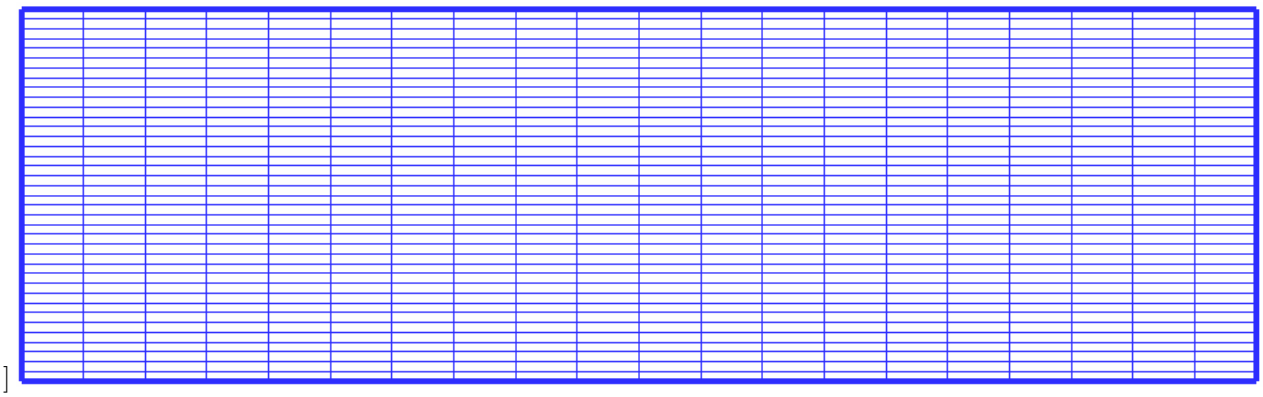

Figure 2. Aerodynamic surface boxes for ZONA6.

III.A. Parametric Dependence

We consider the variation in the flutter boundary due to variations in the structural dimensions of the Goland wing. As mentioned previously, the wing structure is built-up from finite elements which constitute different components of the wing. In order to account for the physical dimensional variation of a manufactured wing we assign one random variable to each wing component. For example, one variable is assigned to all elements which are part of: 1) each of upper and lower wing skins 2) each of the three spars 3) each of the 11 ribs 4) each of the 33 posts. This gives a total of 49 random variables representing each component of the baseline wing model.

III.B. Optimization and Sensitivity Analysis

We study the effect of the wing's structural dimensions on its natural frequencies. A wing design with natural frequencies larger than their baseline values, without increase in baseline weight, is preferred. This optimization problem can be defined as

$$max \quad f_1(\vec{X})$$

subject to:

$$\begin{aligned} &\{f_{m_b}(\vec{X})\} - \{f_{m_d}(\vec{X})\} \leq 0, \qquad m = 2, \ldots, 10 \\ &(1-a)\vec{X_b} \leq \vec{X} \leq (1+a)\vec{X_b}, \\ &\frac{1}{K+M}\left(\sum_{i=1}^{K}\frac{T_i}{T_{i_b}} + \sum_{i=1}^{M}\frac{A_i}{A_{i_b}}\right) \leq 1.0, \end{aligned} \tag{1}$$

where f_1 is the natural frequency of the first mode, subscripts b and d refer to the baseline and designed wings, $\vec{X}$ is the set of design variables which includes thicknesses, T_i (total number K) and areas A_i (total number M), m specifies the natural frequency number m and $a = 50\%$ is a factor used to set the side constraints for the design variables. The last constraint is specified to constrain any increase in the total volume beyond its baseline value.

The sensitivity and optimization analysis were carried out in MSC.Nastran using the method of modified feasible directions. In an initial sensitivity study, all random variables referred to in Section III.A were considered as design variables. The sensitivities of the first 10 natural frequencies to changes in the design variables were computed. Table 3 reports these sensitivities with respect to the fundamental frequency. We note here that the sensitivities change in the post areas are very small. This enabled elimination of 33 random variables for the posts. The final optimization and sensitivity study allowed for spanwise variation of the thickness of the central spar by representing the central spar using 10 design variables from root to tip. Sensitivities of all the resulting 25 variables were significant, with their optimal values listed in Table 4. This wing design is referred to hereafter as designed wing.

Table 3. Sensitivity of first natural frequency to changes in random variables thicknesses.

2-D element	$\delta f_1/\delta T_i$	1-D element	$\delta f_1/\delta A_i$
upper wing skin	$7.5154E+00$	posts[†]	$1.6468E-09$
lower wing skin	$7.5154E+00$		
leading edge spar	$1.9551E+02$	leading edge spar cap	$1.9551E+02$[*]
trailing edge spar	$2.3472E+02$	trailing edge spar cap	$2.3472E+02$
center spar	$5.4847E+00$	center spar cap	$5.4847E+00$
rib 1 (at root)	$0.0000E+00$	rib cap 1 (at root)	$0.0000E+00$
rib 2	$5.4566E-02$	rib cap 2	$5.4566E-02$
rib 3	$3.4048E-02$	rib cap 3	$3.4048E-02$
rib 4	$2.1155E-02$	rib cap 4	$2.1155E-02$
rib 5	$1.1688E-02$	rib cap 5	$1.1688E-02$
rib 6	$5.4300E-03$	rib cap 6	$5.4300E-03$
rib 7	$2.0100E-03$	rib cap 7	$2.0100E-03$
rib 8	$8.7525E-04$	rib cap 8	$8.7525E-04$
rib 9	$1.3086E-03$	rib cap 9	$1.3086E-03$
rib 10	$2.4717E-03$	rib cap 10	$2.4717E-03$
rib 11 (at wing tip)	$1.4195E-03$	rib cap 11 (at wing tip)	$1.4195E-03$

[†] Considered 33 posts, only the largest sensitivity for one of the posts is reported.

[*] Equal sensitivity to the left column indicates same design variable was used for both elements types.

III.C. Monte Carlo Simulation

We use Monte Carlo simulation to propagate variations in the input parameters through the structural and aerodynamic model. Variations in structural dimensions of the wing are inherent to the manufacturing process and are of aleatoric nature (irreducible). We assume that these variations have a Gaussian distribution with nominal values specified in Table 2 for the baseline wing and in Table 4 for the designed wing. In the designed wing, 9 additional random variables are introduced to represent thickness variation of the central spar from root to tip, while excluding the 33 random variables representing the post areas. A heuristic coefficient of variation, $\rho = 0.05$, is assumed for all random variables. A set of 1000 realizations of the structure are then propagated through MSC.Nastran to generate the normal mode shapes. ZAERO® software is then used to carry out the aerodynamic analysis using the ZONA6 method for each realization.

IV. Results

All the linear analyses are carried out using ZAERO® aeroelastic tool. We note here that the ZAERO® flutter module contains two flutter solution techniques: the K-method and the g-method. The g-method is a flutter solution method that generalizes the K-method and the P-K method for true damping prediction. In our analysis, we consider only flutter speeds predicted by the g-method. Furthermore, the flutter analysis is carried out using a non-matched point analysis at a fixed pair of Mach number and density (0.0023771 slugs/feet^3) and various velocities. The free stream conditions are 1° angle of attack and 0 structural damping.

In the following, we conduct a modal sensitivity study to determine the number of vibration modes needed to reliably serve as a backdrop for stochastic analysis, as well as properly describe the transonic flutter bucket. Then we report on the stochastic results which are divided into clean and tip store mass wings. In each case we report on propagated variations first in natural frequencies and second in flutter boundaries. Two configurations of baseline and designed wings are analyzed using ZONA6 aerodynamic analysis tool.

Table 4. Designed wing element sizes: Thicknesses and areas of finite element components.

2-D element	thickness, ft	1-D element	area, ft^2
upper wing skin	0.01710		
lower wing skin	0.01710		
leading edge spar	0.00066	leading edge spar cap†	0.045760
center spar 1 (root)	0.09779	center spar cap 1†(root)	0.164560
center spar 2	0.09779	center spar cap 2	0.164560
center spar 3	0.09779	center spar cap 3	0.164560
center spar 4	0.09779	center spar cap 4	0.164560
center spar 5	0.09779	center spar cap 5	0.164560
center spar 6	0.09779	center spar cap 6	0.164560
center spar 7	0.09779	center spar cap 7	0.164560
center spar 8	0.09779	center spar cap 8	0.164560
center spar 9	0.08001	center spar cap 9	0.134640
center spar 10 (tip)	0.08001	center spar cap 10 (tip)	0.134640
trailing edge spar	0.00066	trailing edge spar†cap	0.045760
rib 1 (at root)	0.03120	rib cap 1‡(at root)	0.037944
rib 2	0.03820	rib cap 2	0.464560
rib 3	0.03820	rib cap 3	0.464560
rib 4	0.03820	rib cap 4	0.464560
rib 5	0.03120	rib cap 5	0.037944
rib 6	0.03120	rib cap 6	0.037944
rib 7	0.03120	rib cap 7	0.037944
rib 8	0.03120	rib cap 8	0.037944
rib 9	0.03120	rib cap 9	0.037944
rib 10	0.03120	rib cap 10	0.037944
rib 11 (at wing tip)	0.03120	rib cap 11 (at wing tip)	0.037944

† Dimension for lower and upper spar caps.

‡ Dimension for lower and upper rib caps.

IV.A. Modal Sensitivity Study

Before considering the modal sensitivity, we note that resolution of flutter boundaries requires selection of an adequate reduced frequency and free stream velocity sets. An initial deterministic study of the flutter boundary (not reported here) found that a reduced frequency set of, k={0.025, 0.075, 0.15, 0.3, 0.5, 0.75, 1.0, 1.2, 1.6, 2.0} and flight speeds, $U = \{300 - 2000\}$ with 20 ft/sec increments were sufficient to define the flutter boundaries.

Modal sensitivity of the flutter boundary of the Goland$^+$ wing is evaluated by computing the boundary using a different number of structural modes $m = \{4, 6, 8, 10\}$ and the ZONA6 aerodynamic method. In all cases, the boundary is compared to ENS3DAE and inviscid CAPTSD results reported by Snyder et al.,[17] where the authors used structural modes only up to $m = 4$. For the clean baseline wing design (see Figure 3a), we observe no significant difference between the boundaries computed by including 4, 6, 8, and 10 modes using the same aerodynamic method. Furthermore, the figure shows that the linear panel method (ZONA6) provides a conservative estimate of the flutter boundary for the subsonic and transonic regimes.

Modal sensitivity of the clean baseline wing with additional tip mass store is reported in Figure 3b. Here some sensitivity, although not significant, is observed for $M = \{0.93, 0.95\}$. Note that as we use a smaller number of structural modes, the flutter boundary becomes less conservative especially at $M = 0.95$. Furthermore, the linear flutter boundary is conservative up to $M = 0.90$, where for $M > 0.90$, ENS3DAE and CAPTSD indicate lower flutter speeds than what is computed using ZONA6.

Because of the relative insensitivity to number of natural modes, $m = \{4, 6, 8, 10\}$, we choose to include all natural modes up to $m = 10$ for carrying the stochastic analysis.

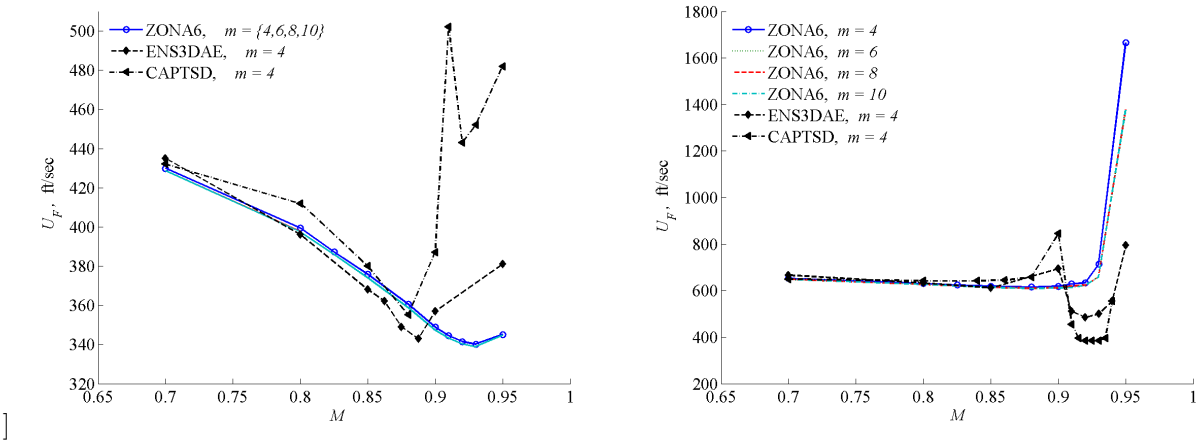

(a) clean wing (b) tip store wing

Figure 3. Deterministic flutter boundary for the baseline wing.

IV.B. Clean Wing

The normal modes frequencies of the 1000 realizations are computed using MSC.Nastran for the clean wing. The normalized histogram and kernel density of the sample distribution for the first, second, third, fourth frequencies, as well as the difference between first and second are reported in Figs.4 and 5 for the baseline and designed wings, respectively. The figures indicate normality of the distribution for all frequencies.

The 1000 modal bases are coupled with the aerodynamic model. The normalized histograms with the kernel density distribution overlaid of the flutter speeds for the clean baseline wing are reported in Figure 6. In the figure we observe that the distributions are approximately normal for all Mach numbers.

The stability boundaries of the sample are reported in Figure 7 for the baseline and designed configurations of the clean wing. In the figure we report the mean flutter speed, $\bar{U}_F$, minimum and maximum outliers, a $\pm 2\sigma$ confidence interval (this corresponds to 95% confidence assuming a normal distribution) and the nominal flutter speed corresponding to unperturbed wing dimensions. The typical transonic dip in the flutter boundary is not observed. This is due to nonapplicability of the method for transonic flight regime. Furthermore, because of the linearity of the method, the $\bar{U}_F$ coincides with $U_F(\vec{X}_b)$.

]

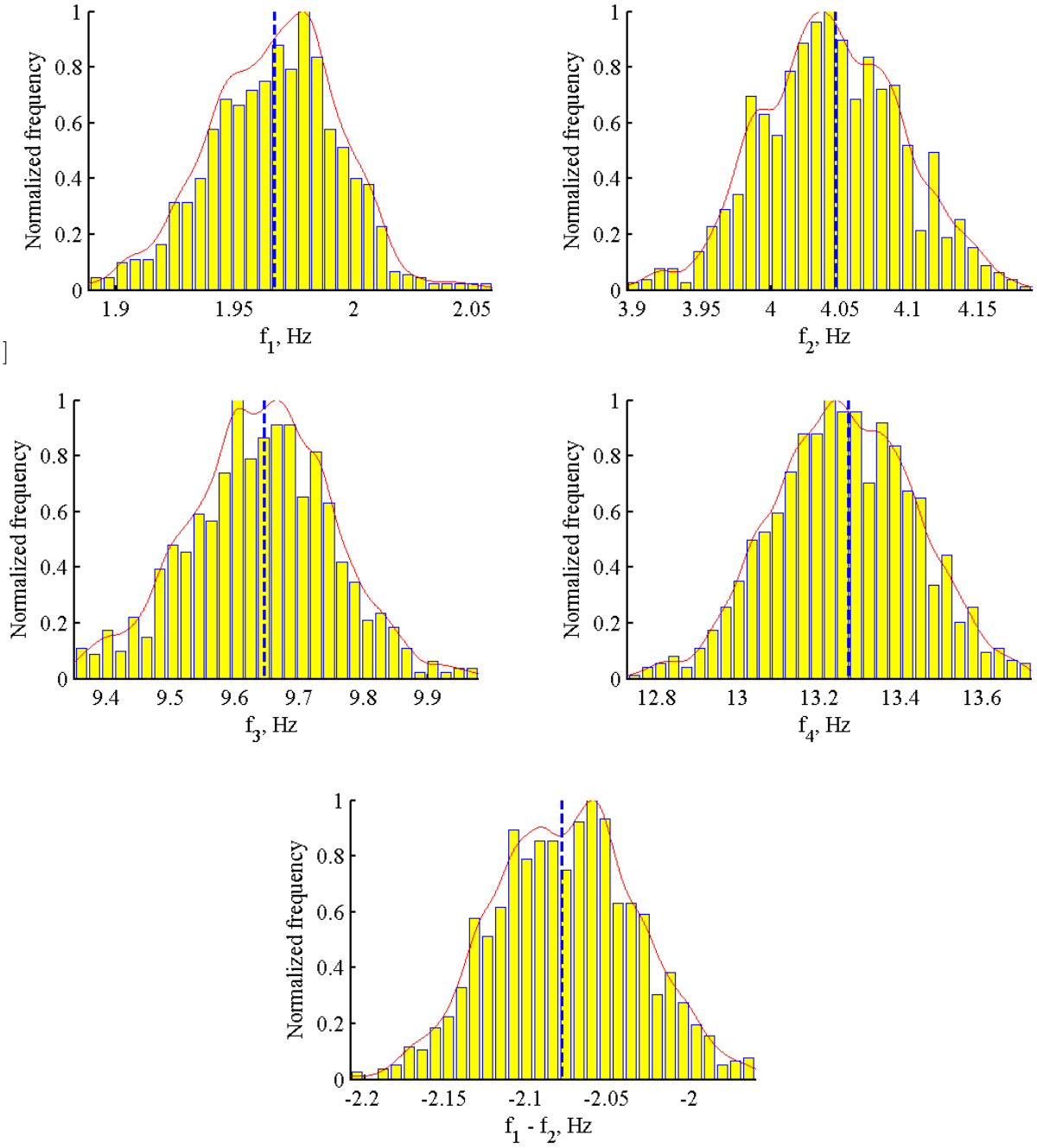

Figure 4. Sample distribution of natural frequencies for first four modes of the clean baseline wing. The frequency of the nominal configuration is indicated by the dashed line.

]

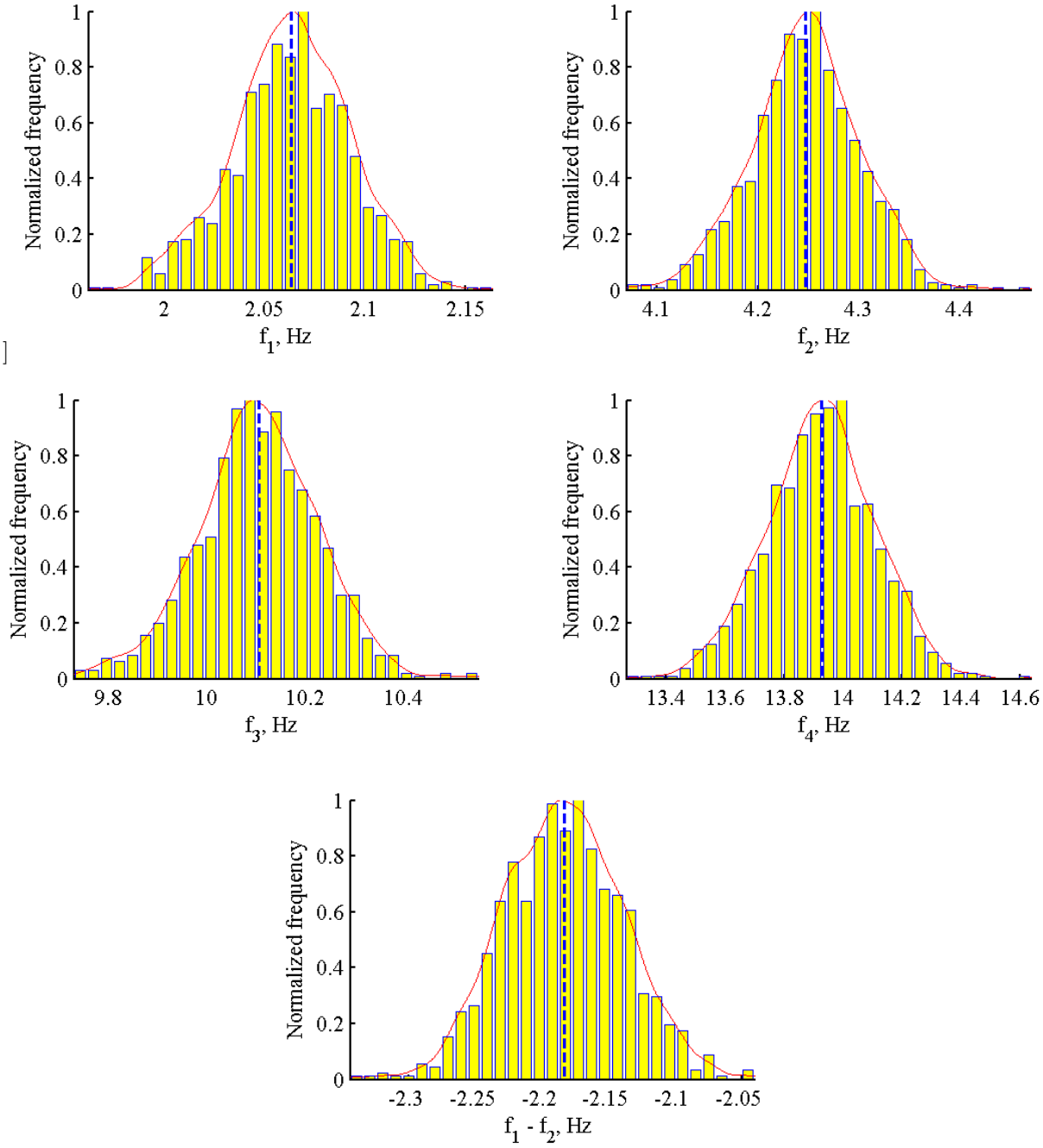

Figure 5. Sample distribution of natural frequencies for first four modes of the clean designed wing. The frequency of the nominal configuration is indicated by the dashed line.

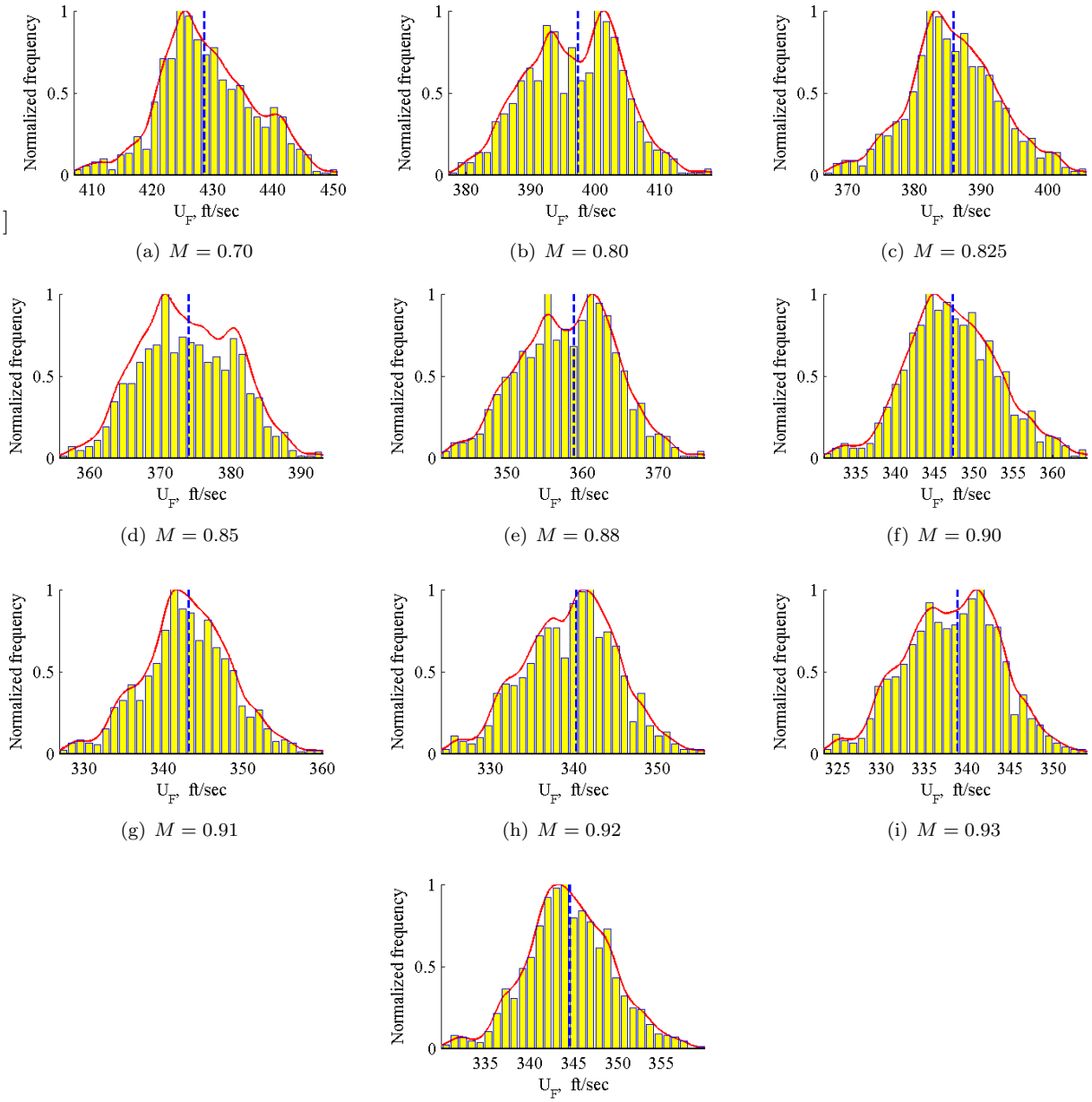

(a) $M = 0.70$ (b) $M = 0.80$ (c) $M = 0.825$

(d) $M = 0.85$ (e) $M = 0.88$ (f) $M = 0.90$

(g) $M = 0.91$ (h) $M = 0.92$ (i) $M = 0.93$

(j) $M = 0.95$

Figure 6. Histogram for ZONA6 CFD analysis of clean baseline wing. The flutter speed of the nominal configuration is noted by the dashed line.

The sample mean and variation are reported in Figure 8. In Figure 8a the mean flutter boundary for the baseline and designed wings are compared. The designed wing configuration exhibits better flutter margin with almost the same values of coefficient of variation as the baseline wing, see Figure 8b. In both the baseline and designed clean wings, it is noteworthy to mention that a structural variation of $\rho = 5\%$ resulted in a variation of $\rho < 3\%$ in the flutter boundary. This highlights the minimal nature of the sensitivity of the boundary to structural variations for the clean wing.

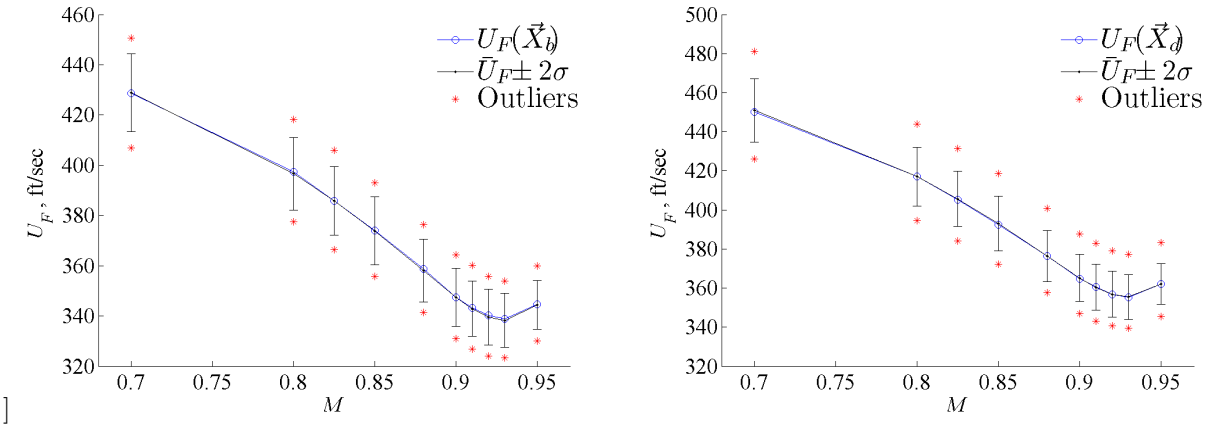

(a) Baseline wing. (b) Designed wing.

Figure 7. Mean and nominal flutter boundary with 95% confidence interval and outliers using Zona6 analysis.

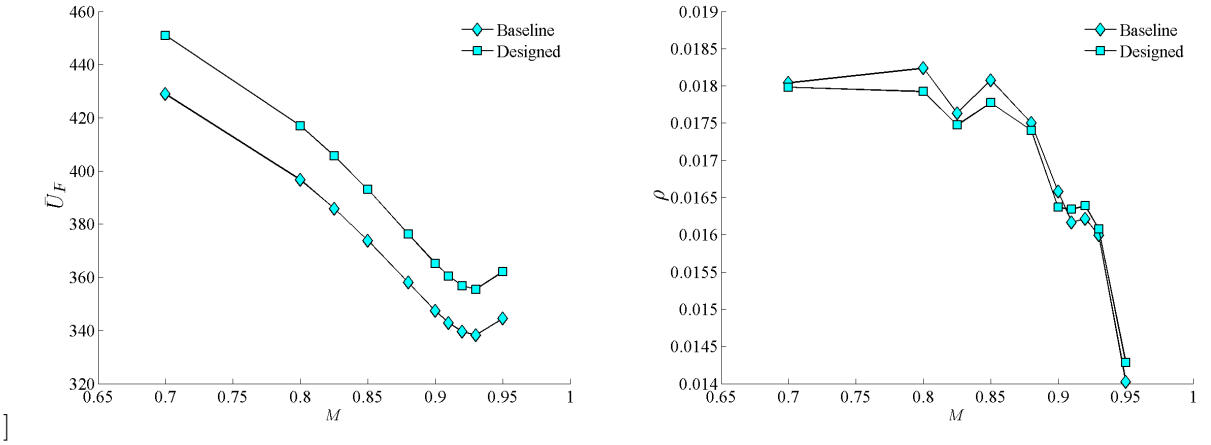

(a) Mean of stability boundary. (b) Coefficient of variation.

Figure 8. Comparison between mean values and coefficient of variation for clean wing.

IV.C. Wing with Tip Store Mass

Results for the wing with tip store mass are presented in the same order as those for the clean wing. The distributions of the normal modes frequencies for the sample are reported in Figures.9 and 11. The distributions are approximately normal for all the natural modes of both the baseline and designed wings. For example, this can be identified for mode 1 by referring to Figure 10a, where the normal probability plot indicates an approximate linear trend.

The initial aerodynamic stochastic results for the baseline and designed wings with tip mass store indicated that the flutter speeds for some structural variations are higher than the maximum flight speed considered in the non-matched point analysis. For these cases, another restart run was performed but with maximum flight speed of $U = 2040$ ft/sec.

The distribution of the flutter speed of the baseline wing at each Mach number are reported in Figure 12 for ZONA6. The distributions are approximately Gaussian up to $M = 0.92$, though at $M = \{0.93, 0.95\}$

]

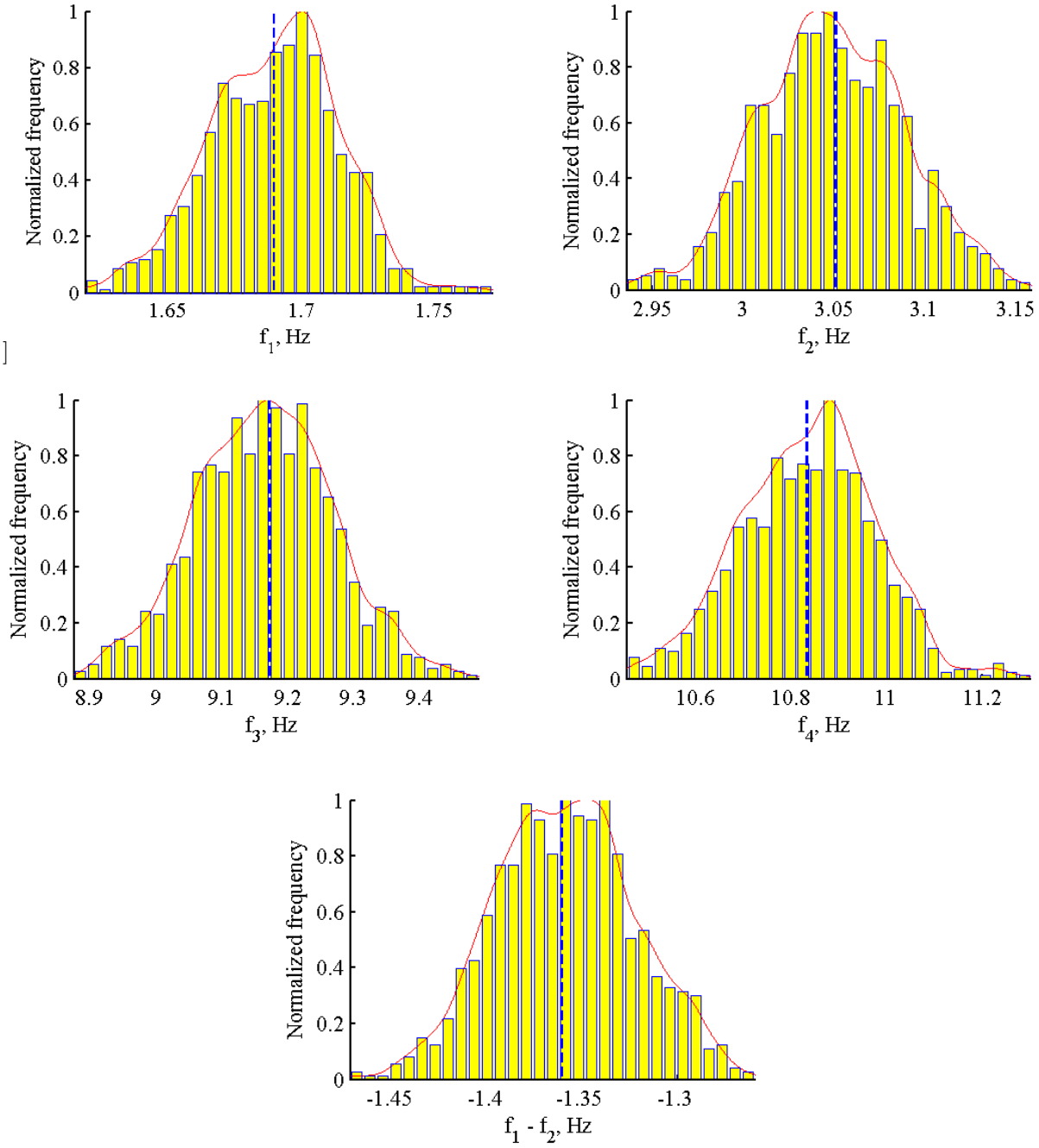

Figure 9. Variations in natural frequencies of first four modes for the baseline wing with tip store mass. The dashed line indicate the natural frequency of the nominal wing configuration.

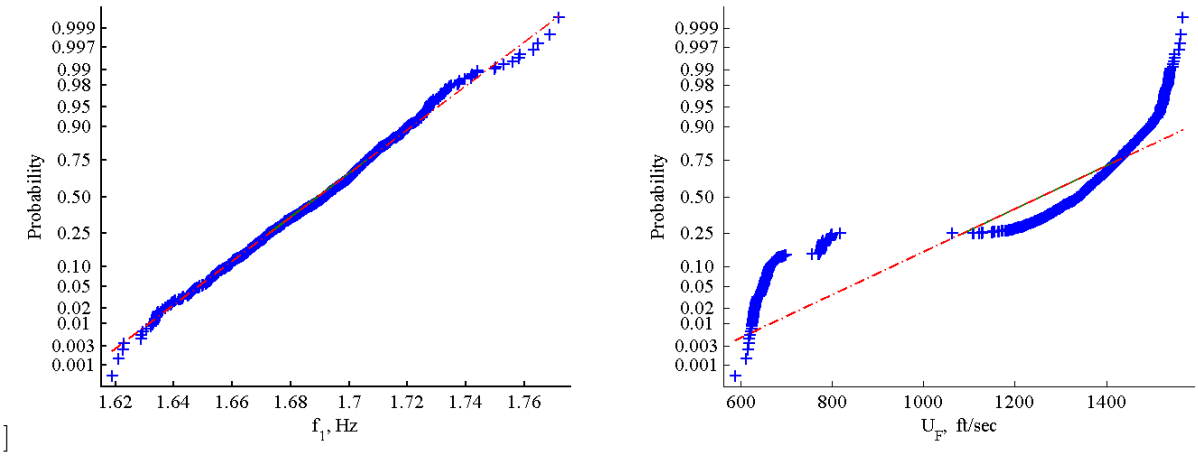

(a) Natural frequency (b) $M = 0.95$

Figure 10. Normal probability plot for the baseline wing with tip store mass.

the distribution becomes tri-modal. The normal probability plot at $M = 0.95$ (see Figure 10b) characterizes this behavior and shows the large deviation from a Gaussian distribution.

The mean, $\pm 2\sigma$ confidence interval and maximum and minimum outliers are reported in Figure 13. High sensitivity to structural variations are noted at $M = \{0.93, 0.95\}$, as shown in Figure 13a. Here $\bar{U}_F$ does not match $U_F(\vec{X}_b)$, and is due to the tri-modal nature of the response distribution observed at these two Mach numbers.

The mean and coefficient of variation are reported in Figure 14. Similar to the clean wing, the mean of the flutter boundary for the designed wing with tip mass exhibits better flutter margin than the baseline one. However, near the transonic flight regime there is high sensitivity to change in Mach number. The coefficient of variation in Figure 14b, although almost identical for both configurations, indicates 8 times more variation in the boundary than the assumed 5% structural variation at $M = 0.93$ and $M = 0.95$. This is mainly due to the high sensitivity of the flutter boundary to structural variations in the transonic flight regime. This large sensitivity was only observed for the tip store mass configuration.

It is worthwhile to study the effect of structural variations on the flutter distribution for different flight altitudes or air densities. Figures 15 and 16 reports these distributions for the baseline wing with tip store for subsonic ($M = 0.70$) and transonic ($M = 0.93$ and $M = 0.95$) flight conditions. The flutter speed for the nominal structural configuration and the mean value of the distribution are additionally reported. At $M = 0.70$, the normality of the distribution is maintained, where the mean value of the boundary continue to increase with altitude. In the transonic regime, the tri-modal form of the distribution at sea level changes to uni-modal as the altitude is increased from 0 ft to 30,000 ft for both $M = 0.93$ and $M = 0.95$. This indicates the vanishing of one of the dominant flutter modes exhibited at sea level and demonstrates the difficulty of setting a flutter margin when there is high sensitivity of the flutter boundary to small changes in the structure. This switching in the flutter modes is shown in Figure 17.

V. Summary and Conclusions

In this work the aeroelastic stability analysis of an ensemble of structural variations of the Goland$^+$ wing with and without tip store mass was analyzed. The ensemble was constructed by applying the Gaussian-distributed variations to the element sizes of the wing's finite element model. To reflect the physical variation in a wing, a random variable was assigned to the respective elements of each wing component. MSC.Nastran was used to compute the mode shapes and the sensitivities of the structural modes frequencies to changes in design variables. The number of random variables was reduced by eliminating the variables with negligible sensitivity. Additionally, an optimization study was conducted to identify a different configuration of the wing which maximizes its first natural frequency. The flutter speeds of the ensemble of structural variations for the baseline and designed wings were computed using linear aerodynamic analysis (ZONA6 module of ZAERO®).

]

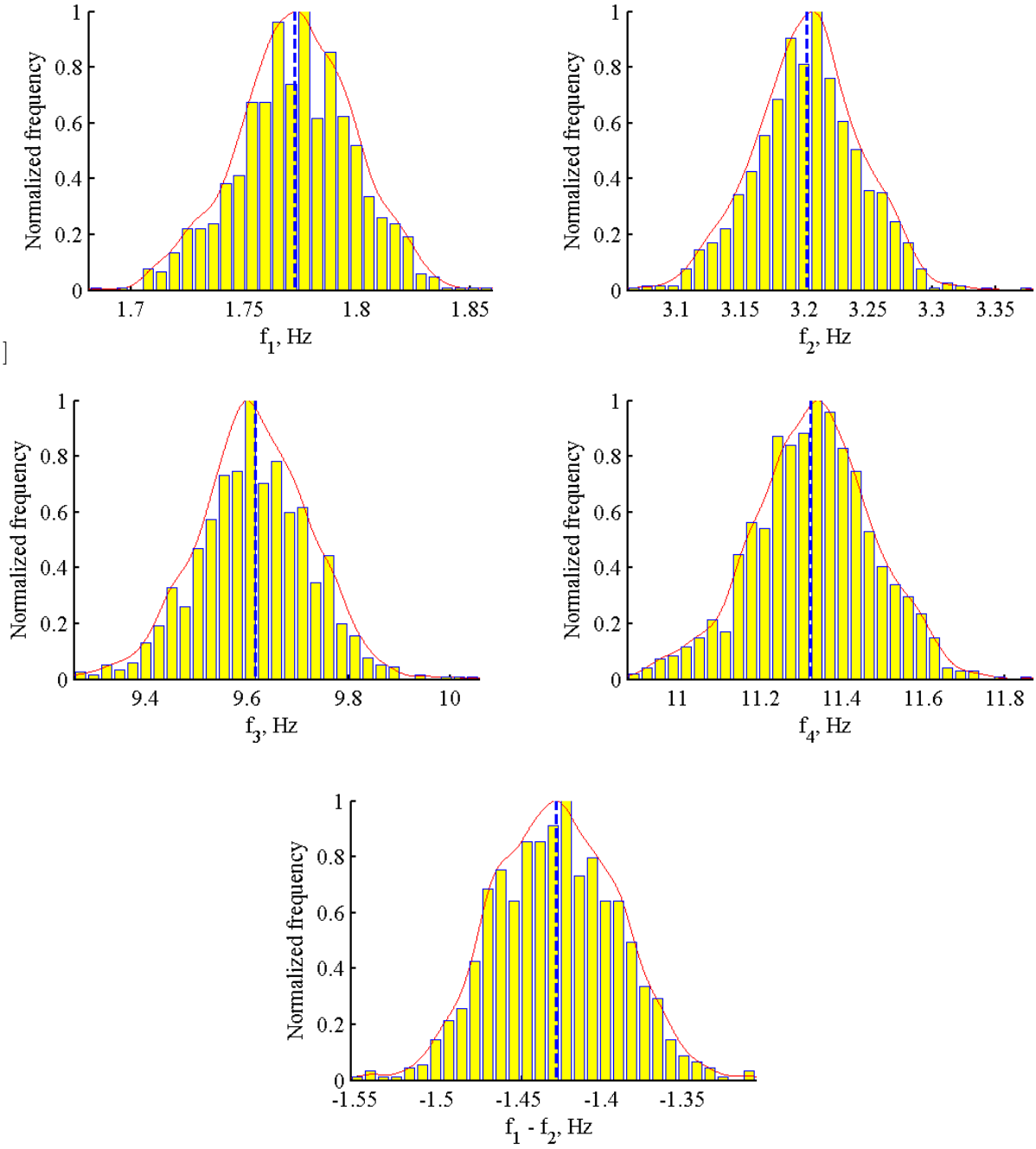

Figure 11. Variations in natural frequencies of first four modes for the designed wing with tip store mass. The dashed line indicate the natural frequency of the nominal wing configuration.

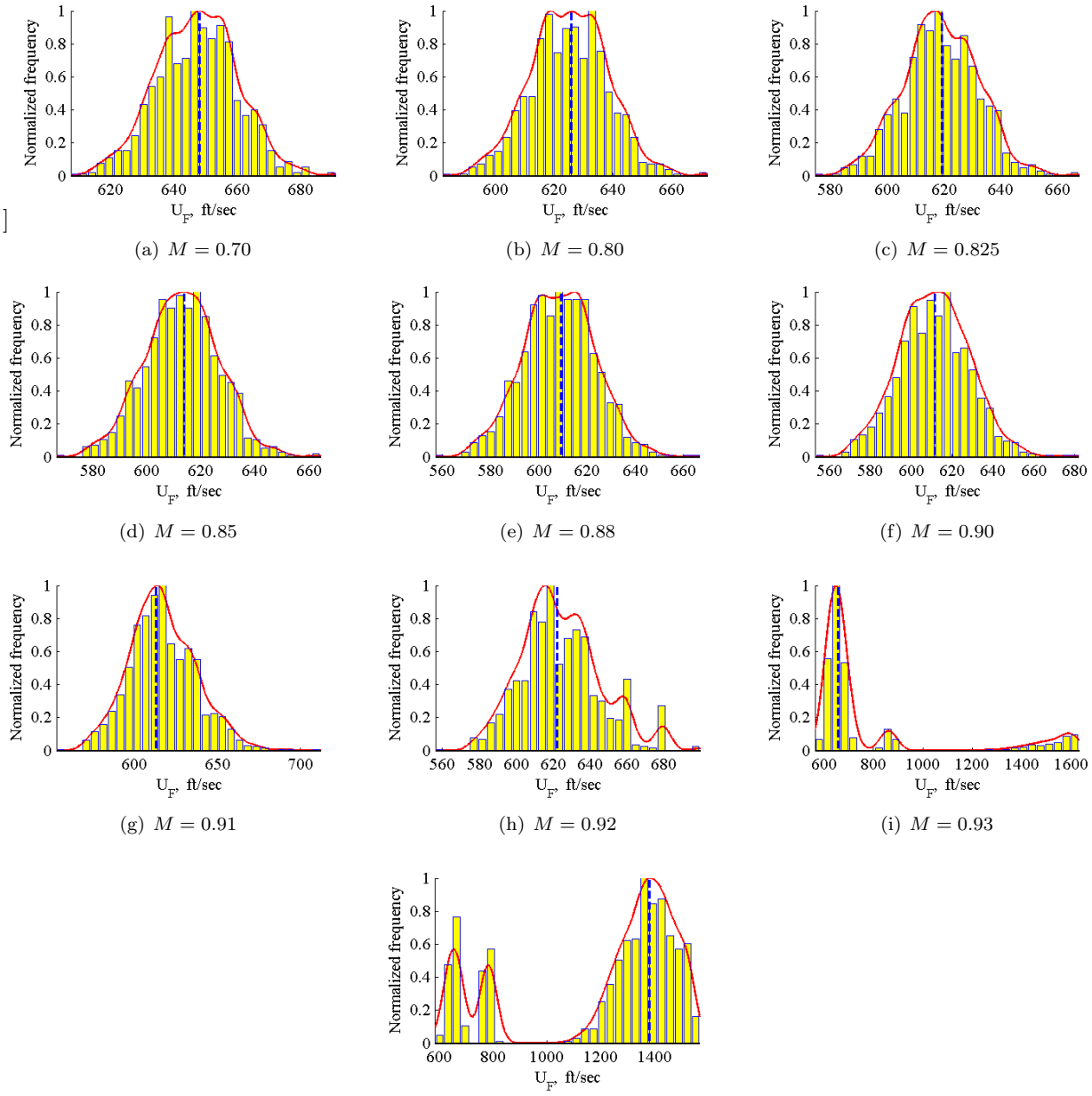

]

(a) $M = 0.70$ (b) $M = 0.80$ (c) $M = 0.825$

(d) $M = 0.85$ (e) $M = 0.88$ (f) $M = 0.90$

(g) $M = 0.91$ (h) $M = 0.92$ (i) $M = 0.93$

(j) $M = 0.95$

Figure 12. Histogram for ZONA6 analysis of baseline wing with additional tip store mass. The dashed line indicate the flutter speed for the nominal structural configuration

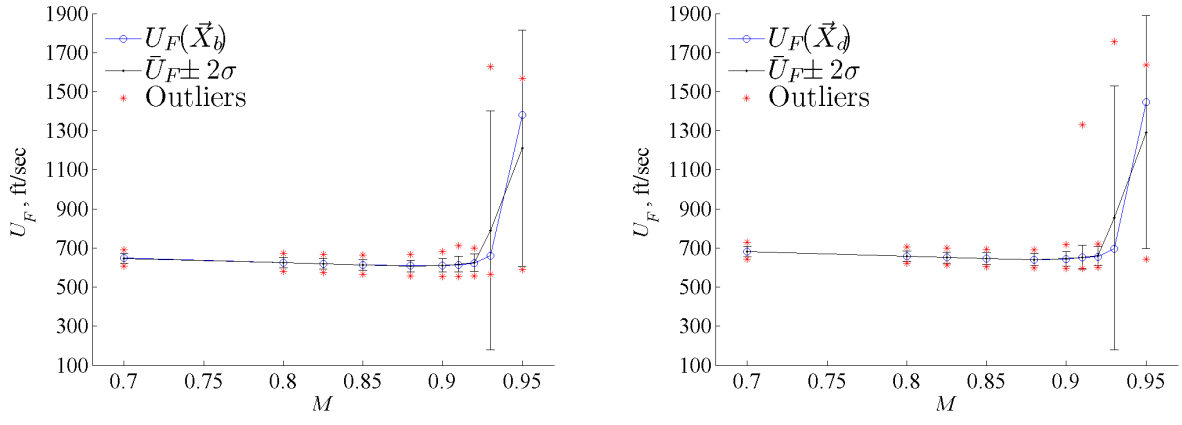

]

(a) Baseline wing (b) Designed wing

Figure 13. Baseline and designed wings with additional tip store mass.

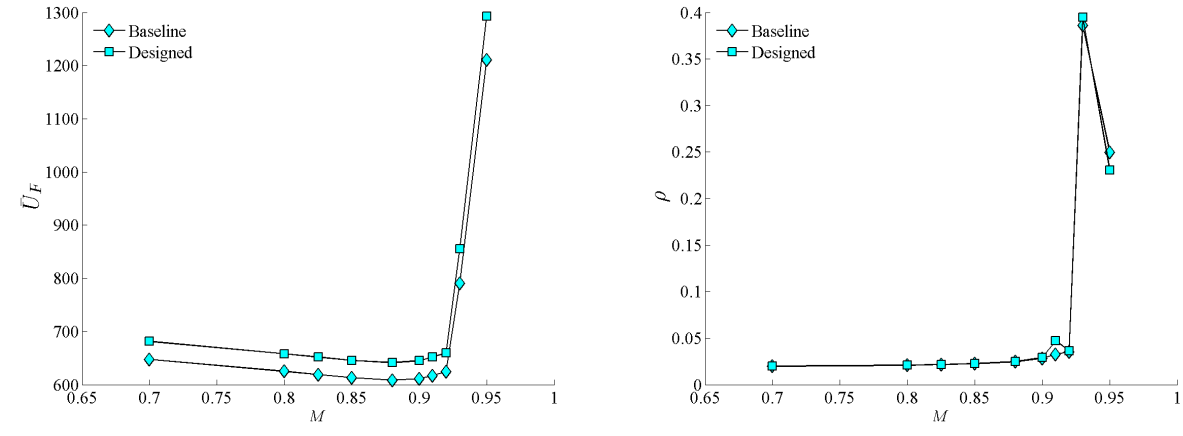

]

(a) Mean of flutter boundary. (b) Coefficient of variation.

Figure 14. Comparison between mean values and coefficient of variation for tip store mass wing.

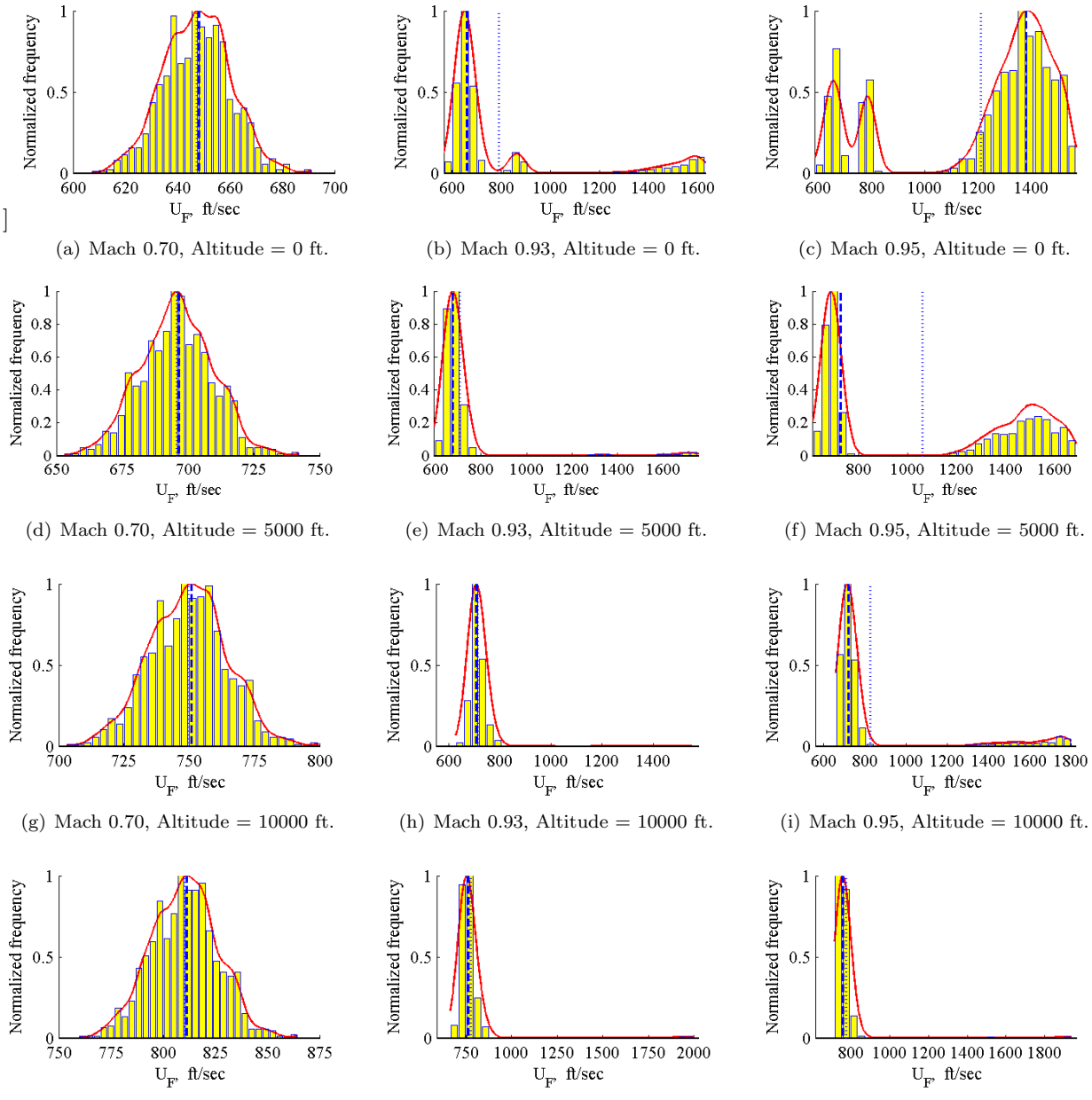

]

(a) Mach 0.70, Altitude = 0 ft.

(b) Mach 0.93, Altitude = 0 ft.

(c) Mach 0.95, Altitude = 0 ft.

(d) Mach 0.70, Altitude = 5000 ft.

(e) Mach 0.93, Altitude = 5000 ft.

(f) Mach 0.95, Altitude = 5000 ft.

(g) Mach 0.70, Altitude = 10000 ft.

(h) Mach 0.93, Altitude = 10000 ft.

(i) Mach 0.95, Altitude = 10000 ft.

(j) Mach 0.70, Altitude = 15000 ft.

(k) Mach 0.93, Altitude = 15000 ft.

(l) Mach 0.95, Altitude = 15000 ft.

Figure 15. Histogram of baseline wing with tip store mass for different altitudes and Mach number. - - Flutter speed for nominal structural configuration; · · · mean flutter speed.

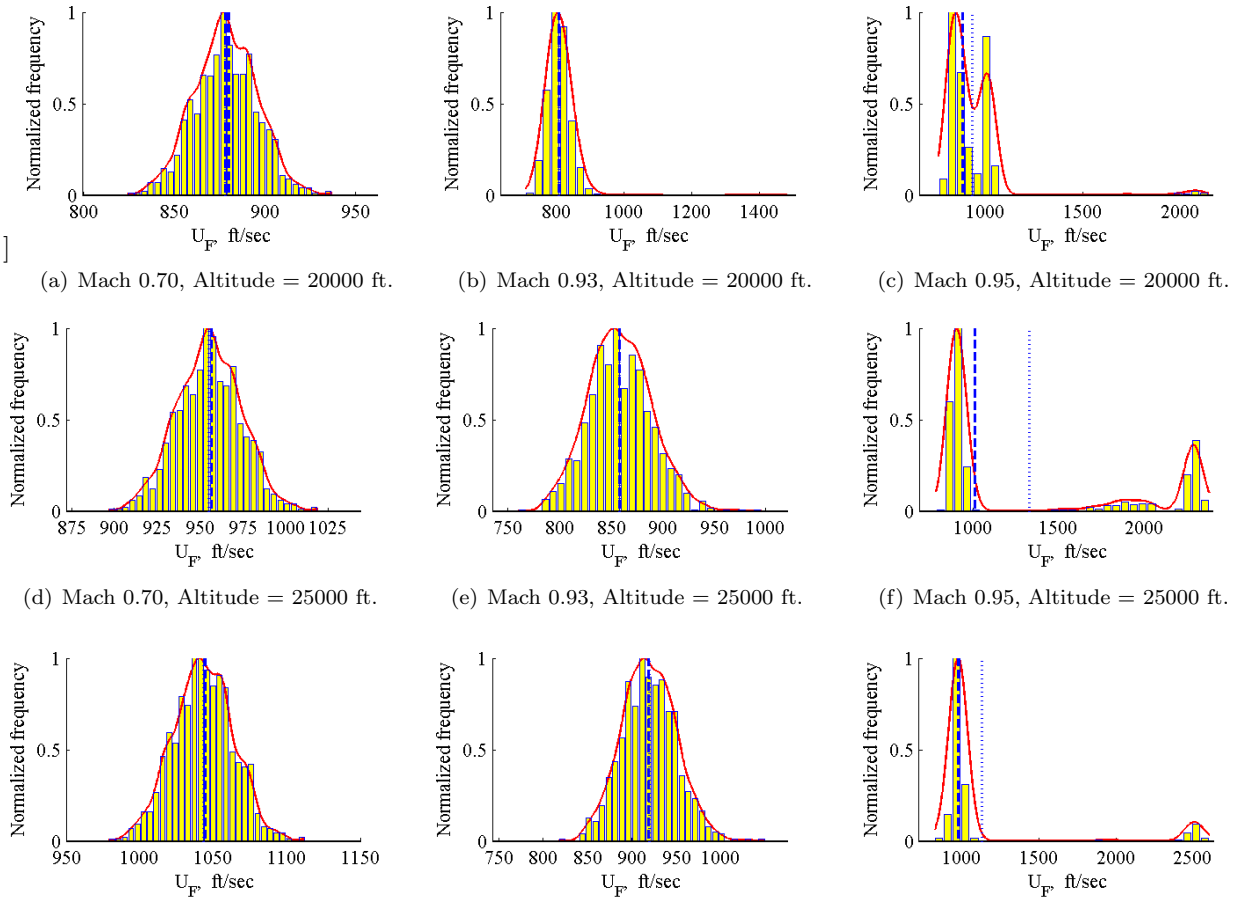

]

(a) Mach 0.70, Altitude = 20000 ft. (b) Mach 0.93, Altitude = 20000 ft. (c) Mach 0.95, Altitude = 20000 ft.

(d) Mach 0.70, Altitude = 25000 ft. (e) Mach 0.93, Altitude = 25000 ft. (f) Mach 0.95, Altitude = 25000 ft.

(g) Mach 0.70, Altitude = 30000 ft. (h) Mach 0.93, Altitude = 30000 ft. (i) Mach 0.95, Altitude = 30000 ft.

Figure 16. Histogram of baseline wing with tip store mass for different altitudes and Mach number. - - Flutter speed for nominal structural configuration; · · · mean flutter speed.

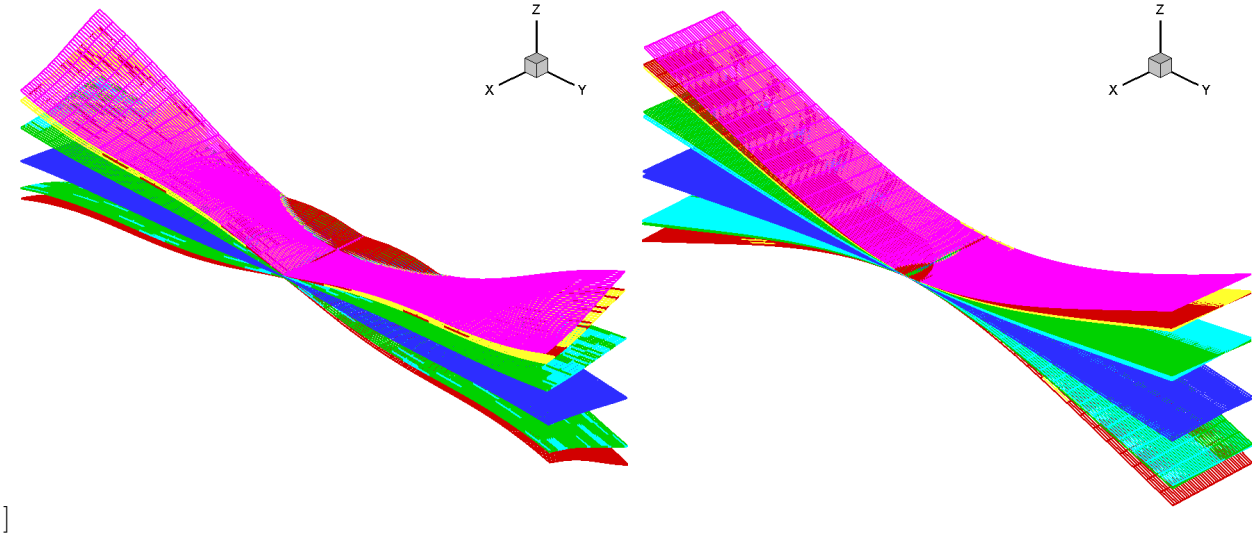

]

(a) Mach 0.95, Altitude = 0 ft, flutter in mode 4. (b) Mach 0.95, Altitude = 10000 ft, flutter in mode 1.

Figure 17. Flutter modes at different altitudes for baseline wing with tip store mass.

The linear aeroelastic analysis of the ensemble of the clean baseline wing (no store mass) did not show high sensitivity of the flutter boundary to small variations in the structure, where the 5% coefficient of variation in the structure only propagated to less than 2% variation in the flutter boundary. Furthermore, the main characteristics of the structural ensemble distribution was maintained in the distribution of the flutter boundary, even in the transonic flight regime. Aeroelastic analysis of the designed wing showed similar distribution characteristics, while improving the flutter margin. However, for the baseline wing configuration with additional tip store mass, high sensitivity of the flutter boundary was observed. This sensitivity was apparent in the transonic flight regime, where the flutter boundary distribution changed its distribution characteristics to bi-modal/tri-modal states. This was mainly attributed to the emergence or disappearance of a flutter mode that degenerates the distribution to a bi-modal or uni-modal one.

The linear analysis was effective in identifying sensitive regions in the flutter boundary of the wing configuration with store mass. This configuration exhibited LCO in previous nonlinear aerodynamic analysis[13] and there is concern of the potential sensitivity when transonic aerodynamics are correctly identified. Such analysis will be exceedingly costly, especially to account for the loss of stability to LCO behavior.

Acknowledgments

The authors would like to thank the National Research Council Research Associateship Program and the Air Force Office of Scientific Research under Grant 03VA01COR (Dr. Fariba Fahroo, Program Manager) for financial and logistical support of the research. The authors would like to thank Dr. Richard Snyder for providing flutter boundary results calculated using ENS3DAE and CAPTSD.

References

[1]Silva, W., Brenner, M., Cooper, J., Denegri, C., Dunn, S., Huttsell, L., Kaynes, I., Lind, R., Poirel, D., and Yurkovich, R., *Collection of Technical Papers - U.S. Air Force T and E Days: Transforming the T and E Enterprise*, Vol. 2005, 2005, pp. 280 – 298.

[2]Ashely, H., "Roles of Shocks in the "Sub-Transonic"Flutter Phenomenon," *Journal of Aircraft*, Vol. 17, 1980, pp. 187–197.

[3]Alonso, J. and Jameson, A., "Fully-Implicit Time-Marching Aeroelastic Solutions," AIAA Paper 1994-0056, January 10-13.

[4]Edwards, J. W., Bennett, R. M., Whitlow, W. J., and Seidel, D. A., "Time-Marching Transonic Flutter Solutions Including Angle-of-Attack Effects," *Journal of Aircraft*, Vol. 20, No. 11, 1983, pp. 899 – 906.

[5]Bendisken, O. and Kousen, K., "Transonic Flutter Analysis Using the Euler Equations," AIAA Paper 87-0911-CP.

[6]Chen, P., Lee, H., and Liu, D., "Unsteady subsonic aerodynamics for bodies and wings with external stores including wake effects," *Journal of Aircraft*, Vol. 30, No. 5, 1993, pp. 618 – 628.

[7]Honda, T. and Antonsson, E., "Preferences and Correlated Uncertanties in Engineering Design," *Proceedings of the ASME Design Engineering Technical Conference*, Vol. 3, Chicago, IL, United States, 2003, pp. 805 – 818.

[8]Becerra, L. and Hernandez, I., "Evaluation of the Air Density Uncertainty: The Effect of the Correlation of Input Quantities and Higher Order Terms in the Taylor Series Expansion," *Measurement Science and Technology*, Vol. 17, No. 10, 2006, pp. 2545.

[9]Kurdi, M., Schmitz, T., Haftka, R., and Mann, B., "Milling Optimization of Removal Rate and Part Accuracy - Part 2: Parameter Variation," *International Journal of Materials Product and Technology*, accepted 2007.

[10]Pettit, C., "Uncertainty Quantification in Aeroelasticity: Recent Results and Research Challenges," *Journal of Aircraft*, Vol. 41, No. 5, 2004, pp. 1217–1229.

[11]Pettit, C. and Ramana, G., "Optimization of a Wing Structure for Gust Response and Aileron Effectiveness," *Journal of Aircraft*, Vol. 40, No. 6, 2003, pp. 1185–1191.

[12]Eastep, F. E. and Olsen, J. J., "Transonic Flutter Analysis of a Rectangular Wing with Conventional Airfoil Sections," *AIAA Journal*, Vol. 17, No. 10, 1980, pp. 1159–1164.

[13]Beran, P., Khot, N., Eastep, F., Snyder, R., and Zweber, J., "Numerical analysis of store-induced limit-cycle oscillation," *Journal of Aircraft*, Vol. 41, No. 6, 2004, pp. 1315 – 1326.

[14]Denegri, C. M., "Limit Cycle Oscillation Flight Test Results of a Fighter with External Stores," *AIAA Journal of Aircraft*, Vol. 37, No. 5, pp. 761–769.

[15]Smith, M., Hodges, D., and Cesnik, C., "An Evaluation of Computational Algorithms to Interface between CFD and CSD Methodologies," WL-TR-96-3055, November 1995.

[16]Smith, M., Schuster, D., Huttsell, L., and Buxton, B., "Development of an Euler/Navier-Stokes Aeroelastic Method for Three-Dimensional Vehicles with Multiple Flexible Surfaces," AIAA Paper 96-1400, April 1996.

[17]Snyder, R., Scott, J., Khot, N., Beran, P., and Zweber, J., "Predictions of Store-Induced Limit-Cycle Oscillations using Euler and Navier-Stokes Fluid Dynamics," AIAA Paper 2003-1727, April 7-10.